

**MODELING OF BLACK LIQUOR GASIFICATION IN A BUBBLING FLUIDIZED BED**

Zumao Chen<sup>a</sup>, Adel F. Sarofim<sup>a,b</sup>, Michael J. Bockelie<sup>a</sup> and Kevin J. Whitty<sup>b</sup>

<sup>a</sup> Reaction Engineering International  
77 West 200 South, Suite 210  
Salt Lake City, UT 84101  
Ph: 801-364-6925  
<http://www.reaction-eng.com>

<sup>b</sup> Department of Chemical and Fuels Engineering  
University of Utah  
1495 East 100 South, Salt Lake City, UT 84112

Black liquor is a byproduct of the chemical pulping process and a critical source of energy for the pulp and paper industry. It contains the spent caustic cooking chemicals and the organic content from the wood liberated during the cooking process. Conventionally, black liquor is incinerated in recovery boilers to recover energy in the form of steam and the cooking chemicals in the form of molten salt. The steam can be used in the mill for heating and drying; it can also be used in a steam turbine to generate electricity. However, recovery boilers are not thermally efficient in comparison with coal or gas fired power generation boilers. Clearly, improvements in efficiency will result in considerable cost savings. Therefore, alternative technologies have attracted increasing interest recently. One such technology is fluidized bed gasification, which has significant advantages over conventional recovery boilers. The product gas of black liquor gasification is a mixture of CO, H<sub>2</sub>, CO<sub>2</sub> and H<sub>2</sub>O, which can be cleaned and burned in a gas turbine or fuel cell to produce electricity, or fired in a boiler to produce process steam for the mill.

In this paper, a three-phase hydrodynamic model has been developed to simulate black liquor gasification in a commercial-scale fluidized bed with horizontal heat exchange tubes. A previously developed probabilistic model is utilized to predict bubble behavior in the tube bundles. The model includes an energy balance for the black liquor particles undergoing gasification within the bed. In addition, the variation of gas mass flow rate, superficial gas velocity and the minimum fluidization velocity is also accounted for. Model calculations compare favorably with available data in terms of the syngas composition and carbon conversion. Further validation of the model is not possible at present due to lack of experimental data. However, work is in progress by other project teams on obtaining data under different operating conditions. Once the data become available, further validation of the model will be carried out and the influence of operating conditions on the performance of the fluidized bed gasifier will be investigated.

## 1. INTRODUCTION

Black liquor is a byproduct of the chemical pulping process. It is a viscous liquid consisting of the spent caustic cooking chemicals and organic lignin removed from wood chips when they are cooked to liberate the fibers that become pulp. Conventional recovery boilers have been used to recover energy from black liquor in the form of steam and the cooking chemicals in the form of molten salt. The steam can be used in the mill for heating and drying; it can also be used in a steam turbine to generate electricity. Recovered chemicals are fed back to the pulping process after several recovery processes. However, the electric power generating efficiency of the recovery boiler system is relatively low, and improvements in power-to-steam ratios will result in considerable cost savings. Therefore, alternative technologies have attracted increasing interest recently. One such technology is fluidized bed gasification, which has significant advantages over the conventional recovery boilers (Grace and Timmer, 1995), including higher energy efficiency and chemical recovery, improved environmental emissions, lower maintenance costs and elimination of the smelt-water explosion hazard. In addition, gasification automatically separates sulfur and sodium in black liquor, which leads to a higher pulp yield and a better pulp quality in the mill. In conventional recovery boilers, nearly all of the sulfur leaves with the molten smelt as sodium sulfide. In black liquor gasification, almost all of the sulfur in black liquor converts to hydrogen sulfide in the syngas, while the sodium leaves the system as sodium carbonate for low-temperature gasification and as molten smelt for high-temperature gasification. Though the fluidized bed technology for black liquor gasification has significant energy and environmental benefits, it is still under development. For a particular system, the hydrodynamics of the fluidized bed is difficult to characterize, especially for the systems with in-bed heat exchange tubes. The gasification behavior of black liquor in the bed also requires additional investigation. To better understand the overall performance of the system, a mathematical model will undoubtedly be beneficial.

Various fluidized bed models have been reported in the literature. These models can be broadly classified into two categories. The first category is the two-phase models; these models assume that the fluidized bed consists of a bubble phase and a dense phase. Different flow patterns may be assumed for the particle phase and the gas phase. However, two-phase models cannot predict gas backmixing in the bed (Fryer and Potter, 1976) and recycle peaks in tracer concentration observed in solids mixing experiments (Lim et al., 1993). The other category is the three-phase models, which represent more realistically the hydrodynamics of the fluidized bed; the models assume that the fluidized bed is comprised of three distinct phases: a bubble phase moving upward and dragging a wake phase behind it and a dense phase in which particles move downward and gas may move upward or downward depending on the superficial gas velocity in the bed.

The overall objective of this paper is to develop a three-phase hydrodynamic model to simulate black liquor gasification in a commercial demonstration fluidized bed in Big Island, Virginia, owned by Georgia-Pacific Corporation. The process employs the MTCI steam reformer technology; the fluidized bed has four indirect PulseEnhanced™ heater bundles, with 253 horizontal tubes each, to provide energy for the endothermic gasification reactions. A schematic of the fluidized bed is shown in Figure 1. Superheated steam and recycled product gas are introduced to the gas distributor with bubble caps. Black liquor is injected at the bottom of the

fluidized bed via dual-fluid injectors to provide uniform distribution of the liquor across the cross-section of the bed. The liquor injector provides a thin film coating of bed particles to enhance gasification and carbon conversion (DeCarrera et al., 2002). A three-phase fluidized bed model has been developed to simulate black liquor gasification in the steam reforming system. The model takes into account the variation of gas mass flow rate, superficial gas velocity and minimum fluidization velocity along the bed height. Gas temperature in different phases is assumed to be the same, however, temperatures of particles in the wake and the dense phases are calculated separately based on energy balance equations. Model predicted syngas composition and carbon conversion are compared with available data.

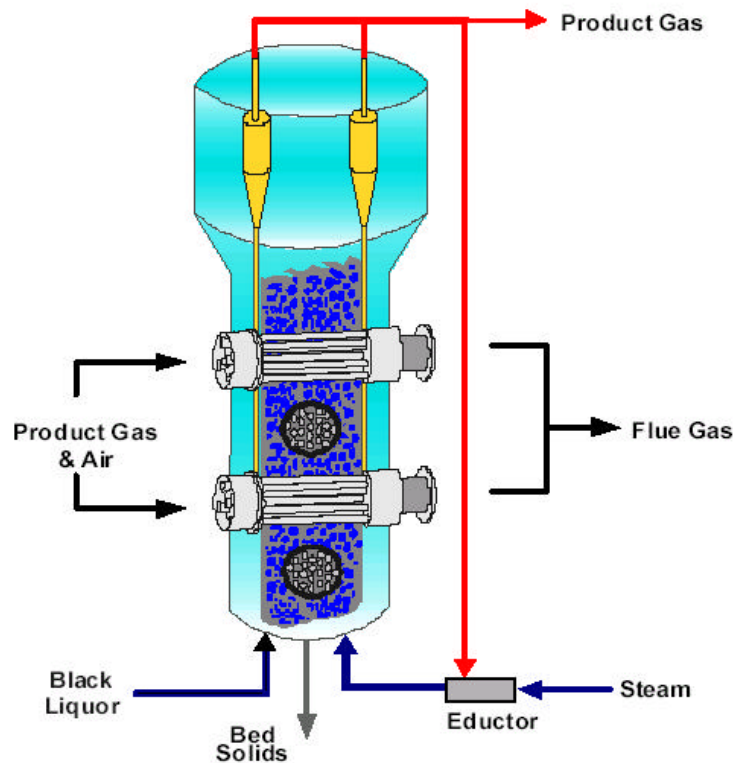


Figure 1. Schematic of the PulseEnhanced™ steam reformer (DeCarrera, et al., 2002).

## 2. BUBBLE HYDRODYNAMICS

### 2.1. Bubble Size

Bubble hydrodynamics in the tube banks differ from that outside the tube banks. With the presence of tube bundles, bubbles interact with the tubes, leading to bubble splitting thereby counteracting the tendency of bubble growth by coalescence. Thus, it is necessary to estimate bubble sizes using different approaches for the regions with and without tube bundles.

### 2.1.1. Regions below and above the tube bundles of the pulse combustors

For three-dimensional fluidized beds, the Darton et al. (1977) correlation has been widely used to predict bubble growth

$$d_b = 0.54(u_0 - u_{mf})^{2/5} (h + 4\sqrt{A_0})^{4/5} / g^{1/5} \quad (1)$$

where  $A_0$  is the catchment area at the distributor plate. For the MTCI process, this is calculated to be  $0.0355 \text{ m}^2$ .

### 2.1.2. Tube bundle regions of the pulse combustors

When bubbles strike tubes, the interaction between the tubes and bubbles may cause bubbles to break up. The size of the daughter bubbles can be predicted using a probabilistic approach developed by Hull et al. (1999). This approach may be summarized briefly as follows.

Assume that the parent bubble has a size,  $d_b$ , less than the horizontal spacing between the tubes,  $L$ . The probability of the parent bubble striking the tube and splitting to form daughter bubbles is  $p = (d_t + d_b)/(d_t + L)$ . The probability of the parent bubble slipping through the horizontal spacing between the tubes without splitting is then  $(1 - p)$ . Assume also that on encounter with the tube, the parent bubble of size  $d_b < L$  breaks up at most into two daughter bubbles of equal size. Therefore, for a three-dimensional bubble,  $d_b^3 = 2d_{b,d}^3$ , where  $d_{b,d}$  is the size of the daughter bubbles. The average size of the bubbles leaving the tube banks,  $d_{b,e}$ , can now be estimated as  $d_{b,e} = pd_{b,d} + (1 - p)d_b$ :

$$\frac{d_{b,e}}{d_b} = 1 - \left(1 - \frac{1}{\sqrt[3]{2}}\right) \left(\frac{d_t + d_b}{d_t + L}\right) \quad \text{for } d_b < L \quad (2)$$

If  $L \leq d_b < d_t + 2L$ , the probability of a bubble encountering two tubes simultaneously is  $p = (d_b - L)/(d_t + L)$ . It is assumed that such an encounter leads to the parent bubble breaking up into three daughter bubbles, one with diameter  $L$ , and the other two daughter bubbles being of equal size. Then,  $d_b^3 = L^3 + 2d_{b,d}^3$  for three-dimensional bubbles. The probability of the parent bubble striking only one tube is  $(1 - p)$ . In this case, the parent bubble splits into two bubbles with equal diameters, thus,  $d_b^3 = 2d_{b,d}^3$ . Using these relationships, the average daughter bubble size is given by

$$d_{b,e} = \frac{d_b}{\sqrt[3]{2}} \left(\frac{d_t + 2L - d_b}{d_t + L}\right) + \frac{L + 2\sqrt[3]{\frac{d_b^3 - L^3}{2}}}{3} \left(\frac{d_b - L}{d_t + L}\right) \quad (3)$$

For  $d_t + 2L \leq d_b < 2d_t + 3L$ , this approach yields

$$d_{b,e} = \frac{L + 2\sqrt[3]{\frac{d_b^3 - L^3}{2}}}{3} \left( \frac{2d_t + 3L - d_b}{d_t + L} \right) + \frac{L + \sqrt[3]{\frac{d_b^3 - 2L^3}{2}}}{2} \left( \frac{d_b - d_t - 2L}{d_t + L} \right) \quad (4)$$

Similarly, for  $d_t + 2L \leq d_b < 2d_t + 3L$ , the daughter bubble size is

$$d_{b,e} = \frac{L + \sqrt[3]{\frac{d_b^3 - 2L^3}{2}}}{2} \left( \frac{3d_t + 4L - d_b}{d_t + L} \right) + \frac{3L + 2\sqrt[3]{\frac{d_b^3 - 3L^3}{2}}}{5} \left( \frac{d_b - 2d_t - 3L}{d_t + L} \right) \quad (5)$$

For  $d_{b,e} \geq 2d_t + 3L$ , equations similar to Equation (5) can be derived. This model has been validated through comparison of model predictions with measurements taken from a thin fluidized bed using a CCD video camera. The applicability of the model to three-dimensional bubbles was also examined. Yates and co-workers (1987, 1990) reported measurements that relate the parent bubble size with the average size of daughter bubbles resulting from encounter with horizontal rows of tubes. Calculations using the above model compared favorably with their experimental data (Hull et al., 1999).

## 2.2. Bubble Rise Velocity

The most frequently adopted two-phase theory shows that bubble rise velocity is the sum of the excess gas velocity and the isolated bubble rise velocity (Davidson and Harrison, 1963)

$$u_b = u_0 - u_{mf} + 0.71\sqrt{gd_b} \quad (6)$$

The excess gas velocity represents the visible bubble flow according to the two-phase theory. Several experimental investigations, however, indicate that the visible bubble flow is somewhat smaller than that predicted by the two-phase theory (Rowe and Yacono, 1976; Werther, 1976). For simplicity, Equation (6) is used in this work.

## 2.3. Bubble Wake Fraction

Bubble wake fraction varies in a wide range as the operating conditions change. Measurements suggest that wake fraction depends on both particle and bubble sizes (Rowe and Partridge, 1965). The scatter in the existing experimental data, however, makes it difficult to use an unequivocal correlation for bubble wake fraction. In the modeling of fluidized beds, it is generally assumed that wake fraction is constant (Chen et al., 2001); in this work, we assume that wake fraction is 0.30.

## 2.4. Bubble Fraction

Based on the assumption that the fluidized bed consists of the bubble phase, wake and dense phases, the overall gas balance can be written as

$$u_0 = f_b u_b + f_b f_w \varepsilon_{mf} u_b + [1 - f_b (1 + f_w)] \varepsilon_{mf} u_{g,d} \quad (7)$$

where  $u_0$  is the local superficial gas velocity and  $u_{g,d}$  is the gas velocity in the dense phase. Since there is not net particle flow in the vertical direction, particles moving upward in the wake phase must be balanced by the downward motion of particles in the dense phase, hence,

$$-f_b u_b f_w = [1 - f_b (1 + f_w)] u_{p,d} \quad (8)$$

where  $u_{p,d}$  is the particle velocity in the dense phase. The slip velocity between the gas and the particles in the dense phase is assumed to be the ratio of the minimum fluidization velocity to the bed voidage at minimum fluidization. Hence, the absolute gas velocity in the dense phase is given by

$$u_{g,d} = u_{p,d} + u_{mf} / \varepsilon_{mf} \quad (9)$$

Equations (7) to (9) can then be employed to determine bubble fraction as a function of bed height. Note that when the superficial gas velocity is sufficiently high,  $u_{g,d}$  may become negative indicating gas in the dense phase moving downward.

### 3. THREE-PHASE BUBBLING FLUIDIZED BED MODEL

A three-phase countercurrent backmixing model has been developed in this work. The model assumes that the fluidized bed consists of three distinct phases:

- A particle-free bubble phase where the gas moves upward in plug flow
- A wake phase where the gas and the solids move upward with the bubbles
- A dense phase in which the solids move downward. The voidage in the dense phase is assumed to be the same as that in the wake phase and is assumed to be the voidage at minimum fluidization

The bubble sizes are calculated allowing for bubble growth by coalescence with increasing height in the bed and decrease in bubble size as a result of bubble intersection with tubes. Different bubble sizes are calculated for the bubbles in the heater tube banks, the voids between the tube banks and the confining cylindrical walls, and the bubbles that flow through the open wedges between the overlap of tube banks. In the model the bubble sizes are averaged across a cylindrical cross section. Details of the model are given in the following sections.

#### 3.1. Overall Gas Balances

Since the total gas mass flow rate may change along the bed height as drying, devolatilization and gasification of black liquor proceed, the superficial gas velocity also changes; it can be written as

$$u_0 = \frac{m_g}{A\rho_g}; \quad m_{g,j} = m_{g,j-1} + \sum_{i=1}^n fR_i M_i Ah \quad (10)$$

where  $j$  is the computational cell index starting from the bottom of the bed;  $f$  is the phase fraction and  $R_i$ ,  $M_i$ , and  $h$  are gas species formation rate ( $\text{kmol}/\text{m}^3\text{s}$ ), species molecular weight and the cell height, respectively.

### 3.2. Species Mass Balances

For steady state conditions, species mass balance equations in different phases can be written as follows:

#### 3.2.1. Bubble phase

$$\frac{d(u_b f_b A C_{i,b})}{dz} - (\lambda_1 C_{i,b} + \lambda_2 C_{i,w}) \frac{d(u_b f_b A)}{dz} + f_b A K_{bw} (C_{i,b} - C_{i,w}) + A f_b R_{i,b} = 0 \quad (11)$$

where  $C_{i,b}$  denotes the concentration of species  $i$ . Subscripts  $b$ ,  $w$  represent the bubble and wake phases, respectively.  $A$  is the cross-sectional area of the bed; it changes along the bed height in the regions of the tube bundles and the freeboard. The first term in the above equation is the convection due to the finite velocity of the bubble phase. The second term represents the cross-flow that accounts for the variation of bubble properties along the bed height above the gas distributor.  $\lambda_1$  and  $\lambda_2$  are constant; if  $d(u_b f_b A)/dz \geq 0$ ,  $\lambda_1 = 0$  and  $\lambda_2 = 1$ ; if  $d(u_b f_b A)/dz < 0$ ,  $\lambda_1 = 1$  and  $\lambda_2 = 0$ . The third term is the exchange of gas between the bubble phase and the wake phase. The last term represents the consumption rate of species  $i$  in the bubble phase.

#### 3.2.2. Wake phase

Similarly, for the wake phase, the gas species mass balance can be written as

$$\begin{aligned} & \frac{d(u_b f_b f_w A \epsilon_{mf} C_{i,w})}{dz} + (\lambda_1 C_{i,b} + \lambda_2 C_{i,w}) \frac{d(u_b f_b A)}{dz} \\ & + (\lambda_3 C_{i,d} + \lambda_4 C_{i,w}) \frac{d\{[1-f_b(1+f_w)]A\epsilon_{mf} u_{g,d}\}}{dz} + f_b K_{bw} A (C_{i,w} - C_{i,b}) \\ & + f_b K_{wd} A (C_{i,w} - C_{i,d}) + f_b f_w \epsilon_{mf} A R_{i,w,g} + f_b f_w (1 - \epsilon_{mf}) A R_{i,w,p} = 0 \end{aligned} \quad (12)$$

The first term in the above equation is the convection term. The second and third terms are the cross-flow.  $\lambda_3$  and  $\lambda_4$  are constant; if  $d\{[1-f_b(1+f_w)]A\epsilon_{mf} u_{g,d}\}/dz \geq 0$ ,  $\lambda_3 = 0$  and  $\lambda_4 = 1$ ; if  $d\{[1-f_b(1+f_w)]A\epsilon_{mf} u_{g,d}\}/dz < 0$ ,  $\lambda_3 = 1$  and  $\lambda_4 = 0$ . The fourth and fifth terms are the exchange of gas between the bubble and wake phases and between the wake and dense phases, respectively. The last two terms represent species consumption rates due to homogeneous and heterogeneous reactions, respectively.

### 3.2.3. Dense phase

For the dense phase, the mass balance equation can be derived as

$$\frac{d\{[1-f_b(1+f_w)]A\epsilon_{mf}u_{g,d}C_{i,d}\}}{dz} - (\lambda_3 C_{i,d} + \lambda_4 C_{i,w}) \frac{d\{[1-f_b(1+f_w)]A\epsilon_{mf}u_{g,d}\}}{dz} + f_b K_{wd}A(C_{i,d} - C_{i,w}) + [1-f_b(1+f_w)]A\epsilon_{mf}R_{i,d,g} + \{1-f_b(1+f_w)\}A(1-\epsilon_{mf})R_{i,d,p} = 0 \quad (13)$$

The terms in the above equation represent convection, cross-flow, exchange of gas between the dense and wake phases, species consumption rates due to homogeneous and heterogeneous reactions, respectively.

### 3.2.4. Freeboard region

In the freeboard, homogeneous reactions, especially the water-gas shift reaction and the methane-steam reforming reaction, continue. The mass balance equation must account for these reactions. The species mass balance equation is

$$u_0 \frac{dC_{i,f}}{dz} + R_{i,f} = 0 \quad (14)$$

## 3.3. Exchange Coefficients

The mass exchange coefficients have been adopted from Kunii and Levenspiel (1991). The mass transfer coefficient between the bubble phase and the wake phase is

$$K_{bw} = 5.85(D_g^{0.5}g^{0.25}/d_b^{1.25}) + 4.5u_{mf}/d_b \quad (15)$$

where  $D_g$  is the gas diffusivity and  $d_b$  is the bubble diameter. The mass exchange coefficient between the wake and emulsion phases is taken as

$$K_{wd} = 6.77(0.71\sqrt{gd_b}D_g\epsilon_{mf}/d_b^3)^{1/2} \quad (16)$$

## 3.4. Energy Balance

Assume the gas in the bubble phase, the wake phase and the dense phase has the same temperature. An energy balance for the gas phase can be written as

$$C_{pg}\rho_g u_0 \frac{dT_g}{dz} + \frac{6h_w}{d_p} f_b f_w (1-\epsilon_{mf})(T_g - T_{p,w}) + \frac{6h_d}{d_p} [1-f_b(1+f_w)](1-\epsilon_{mf})(T_g - T_{p,d}) + f_b \sum_{i=1}^n (-\Delta H_{i,b})R_{i,b} + f_b f_w \epsilon_{mf} \sum_{i=1}^n (-\Delta H_{i,w,g})R_{i,w,g} + [1-f_b(1+f_w)]\epsilon_{mf} \sum_{i=1}^n (-\Delta H_{i,d,g})R_{i,d,g} + Q_t = 0 \quad (17)$$

where  $d_p$  is the particle diameter;  $h_w$  and  $h_d$  are the heat transfer coefficients between the gas and the particles in the wake phase, and between the gas and the particles in the dense phase, respectively, and can be readily estimated using correlations given in Kunii and Levenspiel (1991). The first term in the above equation arises due to particle motion. The second term represents the convective heat transfer between the gas in the wake phase and the solids in the wake phase. Similarly, the third term accounts for the convective transfer between the gas in the dense phase and the solids in the dense phase. The fourth, fifth and sixth terms represent the gas phase reactions in the bubble phase, the wake phase and the dense phase, respectively. The last term is the heat transferred to the bed from the pulse combustors. Similarly, for the particles in the wake phase, the energy balance equation can be derived as

$$\begin{aligned}
& C_{pp}\rho_p(1-\varepsilon_{mf})\frac{d(u_b f_b f_w A T_{p,w})}{dz} + C_{pp}\rho_p f_b f_w A K_{wd,p}(T_{p,w} - T_{p,d}) \\
& - C_{pp}\rho_p(1-\varepsilon_{mf})(\lambda_5 T_{p,w} + \lambda_6 T_{p,d})\frac{d(u_b f_b f_w A)}{dz} \\
& + f_b f_w A(1-\varepsilon_{mf})\left\{\frac{6h_w}{d_p}(T_{p,w} - T_g) + \sum_{i=1}^n (-\Delta H_{i,w,s})R_{i,w,p}\right\} + A Q_{vap} = 0
\end{aligned} \tag{18}$$

where  $Q_{vap}$  is the energy required to vaporize the water in the black liquor. The second term accounts for the heat transfer due to the solids exchange between the wake phase and the dense phase. The fourth term represents heat exchange between the solids and the gas in the wake phase and the energy consumption due to the heterogeneous reactions in the wake phase. Other terms are similar to those in the previous equations. Similar energy balance equation can be written for the particles in the dense phase,

$$\begin{aligned}
& C_{pp}\rho_p(1-\varepsilon_{mf})\frac{d\{u_{p,d}[1-f_b(1+f_w)]AT_{p,d}\}}{dz} + C_{pp}\rho_p f_b f_w A K_{wd,p}(T_{p,d} - T_{p,w}) \\
& + C_{pp}\rho_p(1-\varepsilon_{mf})(\lambda_5 T_{p,w} + \lambda_6 T_{p,d})\frac{d(u_b f_b f_w A)}{dz} \\
& + [1-f_b(1+f_w)]A(1-\varepsilon_{mf})\left\{\frac{6h_d}{d_p}(T_{p,d} - T_g) + \sum_{i=1}^n (-\Delta H_{i,d,p})R_{i,d,p}\right\} = 0
\end{aligned} \tag{19}$$

Assume that there is not heat exchange between the gas phase and the reactor wall in the freeboard, the energy balance for the freeboard is then given by

$$u_0 C_{pg}\rho_g \frac{dT_g}{dz} + \sum_{i=1}^n (-\Delta H_{i,f})R_{i,f} = 0 \tag{20}$$

The second term represents heat of reactions due to the homogeneous reactions.

### 3.5. Boundary Conditions

The boundary conditions for the energy balance equations are: at the bottom of the bed,

$$T_g = T_{g,\text{inlet}}; T_{p,w} = \frac{m_p T_{p0} - [1 - f_b(1 + f_w)](1 - \epsilon_{mf})u_{p,d}A\rho_p T_{p,d}}{f_b f_w u_b (1 - \epsilon_{mf})A\rho_p} \quad \text{at } z = 0 \quad (21)$$

at the top surface of the fluidized bed,

$$T_{p,d} = T_{p,w} \quad \text{at } z = H_t \quad (22)$$

The boundary conditions for the mass balance equations depend on the direction of the gas flow in the dense phase. If  $u_{g,e} > 0$  at  $z = 0$ , then, at the gas distributor,

$$C_{i,b} = C_{i,w} = C_{i,d} = C_{i,\text{inlet}} \quad \text{at } z = 0 \quad (23)$$

However, if  $u_{g,d} < 0$  at  $z = 0$ , then, at the bottom of the bed,

$$C_{i,b} = C_{i,\text{inlet}}; C_{i,w} = \frac{(u_0 - f_b u_b)C_{i,\text{inlet}} - [1 - f_b(1 + f_w)]\epsilon_{mf} u_{g,e} C_{i,e}}{f_b f_w \epsilon_{mf} u_b} \quad \text{at } z = 0 \quad (24)$$

and at the top of the bed,

$$C_{i,d} = C_{i,w} \quad \text{at } z = H_t \quad (25)$$

### 3.6. Drying and Devolatilization of Black Liquor

Experimental data show that drying and devolatilization of black liquor are heat transfer controlled processes under recovery furnace conditions (Frederick, 1990). Experiments and model simulations also indicate that, under these conditions, drying and devolatilization take place simultaneously as black liquor droplets are heated (Dayton and Frederick, 1995; Verrill and Wessel, 1995). However, under the conditions considered here, it is expected that drying and devolatilization occur consecutively. It is assumed that devolatilization takes place only after the droplets are completely dry. The energy balance for a single black liquor droplet can be written as

$$C_{pp}\rho_p \frac{dT_p}{dt} = \frac{6h_w}{d_p}(T_g - T_p) - m_{\text{vap}}\lambda_{\text{vap}} \quad (26)$$

where  $m_{\text{vap}}$  is the volumetric evaporation rate ( $\text{kg}/\text{m}^3\text{s}$ ) of black liquor water and  $\lambda_{\text{vap}}$  is the latent heat of evaporation. If drying is a heat transfer controlled process, black liquor droplets can then be assumed to be at pseudo-steady state, thus,

$$m_{\text{vap}} = \frac{6h_w}{d_p \lambda_{\text{vap}}} (T_g - T_p) \quad (27)$$

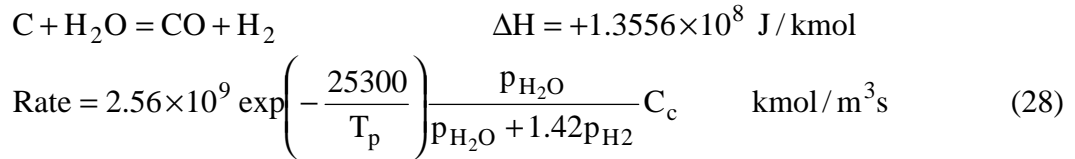
where  $T_g$  is the local gas temperature. Droplet temperature,  $T_p$ , can be assumed to be the temperature of the boiling point of water at the local pressure. Drying begins once black liquor enters the fluidized bed and is complete when all the water in black liquor vaporizes.

For simplicity, it is assumed that devolatilization time is the same as that of drying. The fraction of each component in black liquor released into the gas phase depends on the environmental temperature to which the black liquor subjects. Correlations reported in Frederick and Hupa (1993) and Frederick et al. (1995) are used to determine C, H, O and S release rates. Volatiles are assumed to consist of  $\text{CH}_4$ ,  $\text{CO}$ ,  $\text{H}_2\text{O}$  and  $\text{H}_2\text{S}$ . The release amount of each gas species can be determined from the element mass balance.

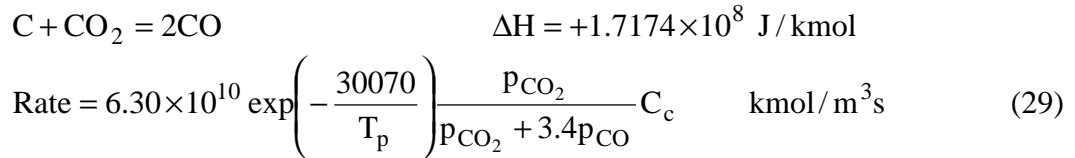
### 3.7. Gasification Kinetics

Global reaction mechanisms are used to describe black liquor gasification. The reactions considered in the model include:

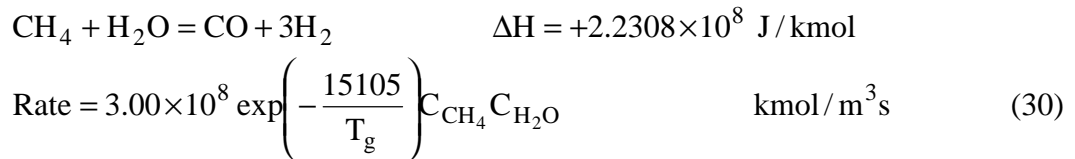
**Steam gasification** (Li and van Heiningen, 1991)



**$\text{CO}_2$  gasification** (Li and van Heiningen, 1990)



**Methane-steam reforming reaction** (Jones and Lindstedt, 1988)



Kinetics for other reactions have been adopted from MFIX (Guenther et al., 2002), which is a modified version of the reaction scheme used in Syamlal and Bissett (1992), and is based on gasification kinetics proposed by Wen et al. (1982).

**Methanation** (Wen et al., 1982; Syamlal and Bissett, 1992)

$$\begin{aligned}
\text{C} + 2\text{H}_2 &= \text{CH}_4 & \Delta H &= -8.7519 \times 10^7 \text{ J/kmol} \\
\text{Rate} &= 9.87 \times 10^{-6} \exp\left(-7.087 - \frac{8078}{T_p}\right) (p_{\text{H}_2} - p_{\text{H}_2}^*) C_c & \text{kmol/m}^3\text{s} & \quad (31)
\end{aligned}$$

where

$$p_{\text{H}_2}^* = \sqrt{\frac{1.01325 \times 10^5 p_{\text{CH}_4}}{\exp(-13.43 + 10999/T_p)}} \quad (32)$$

**Carbon combustion** (Wen et al., 1982; Syamlal and Bissett, 1992)

$$\begin{aligned}
\text{C} + \frac{1}{2}\text{O}_2 &= \text{CO} & \Delta H &= -1.1129 \times 10^8 \text{ J/kmol} \\
\text{Rate} &= \frac{5.9215 \times 10^{-4} p_{\text{O}_2}}{d_p \left( \frac{1}{k_f} + \frac{1}{k_r} \right)} & \text{kmol/m}^3\text{s} & \quad (33)
\end{aligned}$$

where the film resistance is given by

$$k_f = \frac{100 D_{\text{O}_2} \text{Sh}}{d_p R_{\text{O}_2} T_f} \quad (34)$$

where  $R_{\text{O}_2}$  is the gas constant for oxygen,  $R_{\text{O}_2} = 0.25982 \text{ m}^3 \cdot \text{Pa} / \text{g} \cdot \text{K}$ ;  $T_f$  is the film temperature and can be calculated as

$$T_f = (T_g + T_p) / 2 \quad (35)$$

The Sherwood number is given by (Gunn, 1978)

$$\text{Sh} = (7 - 10 \epsilon_g + 5 \epsilon_g^2) (1 + 0.7 \text{Re}^{0.2} \text{Sc}^{1/3}) + (1.33 - 2.4 \epsilon_g + 1.2 \epsilon_g^2) \text{Re}^{0.7} \text{Sc}^{1/3} \quad (36)$$

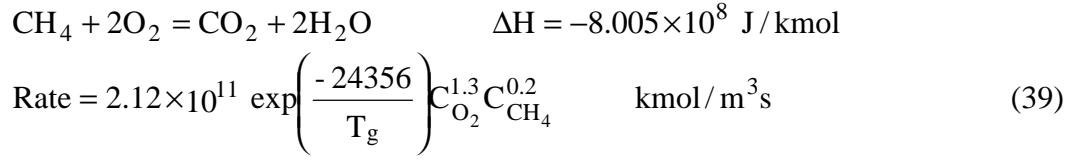
The surface reaction rate is given by (Desai and Wen, 1978)

$$k_r = 860 \exp\left(-\frac{13587}{T_p}\right) \text{ g/Pa} \cdot \text{m}^2 \cdot \text{s} \quad (37)$$

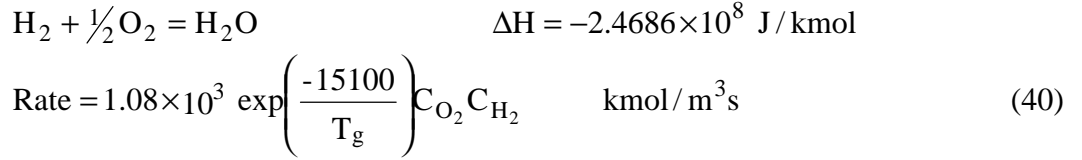
**CO combustion** (Westbrook and Dryer, 1981)

$$\begin{aligned}
\text{CO} + \frac{1}{2}\text{O}_2 &= \text{CO}_2 & \Delta H &= -2.8303 \times 10^8 \text{ J/kmol} \\
\text{Rate} &= 2.238 \times 10^{12} \exp\left(-\frac{20130}{T_g}\right) C_{\text{O}_2}^{0.25} C_{\text{CO}} C_{\text{H}_2\text{O}}^{0.5} & \text{kmol/m}^3\text{s} & \quad (38)
\end{aligned}$$

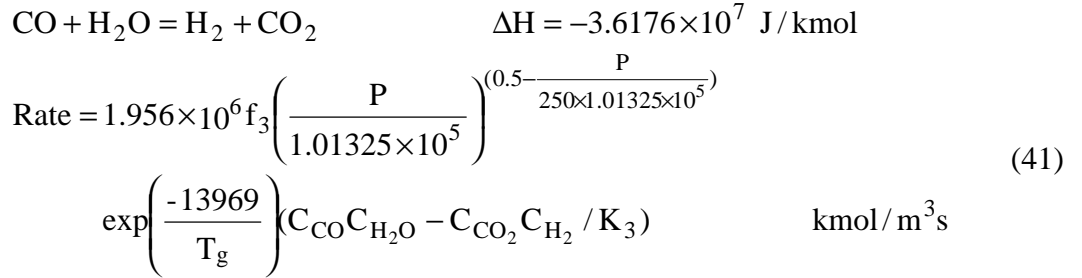
**CH<sub>4</sub> combustion** (Westbrook and Dryer, 1981)



**H<sub>2</sub> combustion** (Peters, 1979)



**Water-gas shift reaction** (Wen et al., 1982)



where

$$f_3 = 10^{-3} \exp(-8.91 + 5553/T_g) C_{\text{ash}} \quad (42)$$

and the equilibrium constant is given by

$$K_3 = \exp(-3.63061 + 3955.71/T_g) \quad (43)$$

The reactions involving oxygen are insignificant since for the system considered here, there is not oxygen in the inlet streams or oxygen formed in the bed; however, these reactions are included so that the computer code developed may also be used for combustion of black liquor. The above mechanisms only account for gasification and combustion of carbon in black liquor. Since black liquor contains significant amount of oxygen and considerable amount of hydrogen, it is important to also consider the release of elemental oxygen and hydrogen from black liquor during gasification. It is assumed that ash consists of sodium carbonate and potassium carbonate. The release rates of elemental oxygen and hydrogen are assumed to be proportional to the carbon gasification/combustion rate and the ratio of the amount of elemental oxygen or hydrogen available for release to the amount of carbon available for gasification. Elemental oxygen and elemental hydrogen are assumed to release as water vapor and hydrogen or carbon monoxide depending on the relative release rates of elemental oxygen and hydrogen.

#### 4. MODEL RESULTS

The mass and energy balance equations given above form a set of equations, which have to be solved numerically simultaneously along with the boundary conditions. A finite-difference method has been used to discretize the equations and a computer code has been developed. In order to test the code, the following operating conditions are used in the simulations:

- Black liquor solids: 8300 lb/hr
- Liquor solids mass fraction: 0.59
- Steam flow rate: 6850 lb/hr
- Recycle gas: 4170 lb/hr
- Pressure at the freeboard: 8.8 psig
- Solids removal rate: 2835 lb/hr
- Pulse combustor energy input: 6.0 MW

Figure 2 represents model predicted syngas composition in comparison with the design syngas composition and results from a model, denoted as UU model in the figure, developed by Whitty (2003). Whitty divided the fluidized bed into ten sections, and in each section, he assumed 10% of black liquor gasified completely. It can be seen that the present model predictions compare reasonably with other data. In addition, Georgia-Pacific reports a carbon conversion of above 95%; our model predicts a carbon conversion of 99.6%.

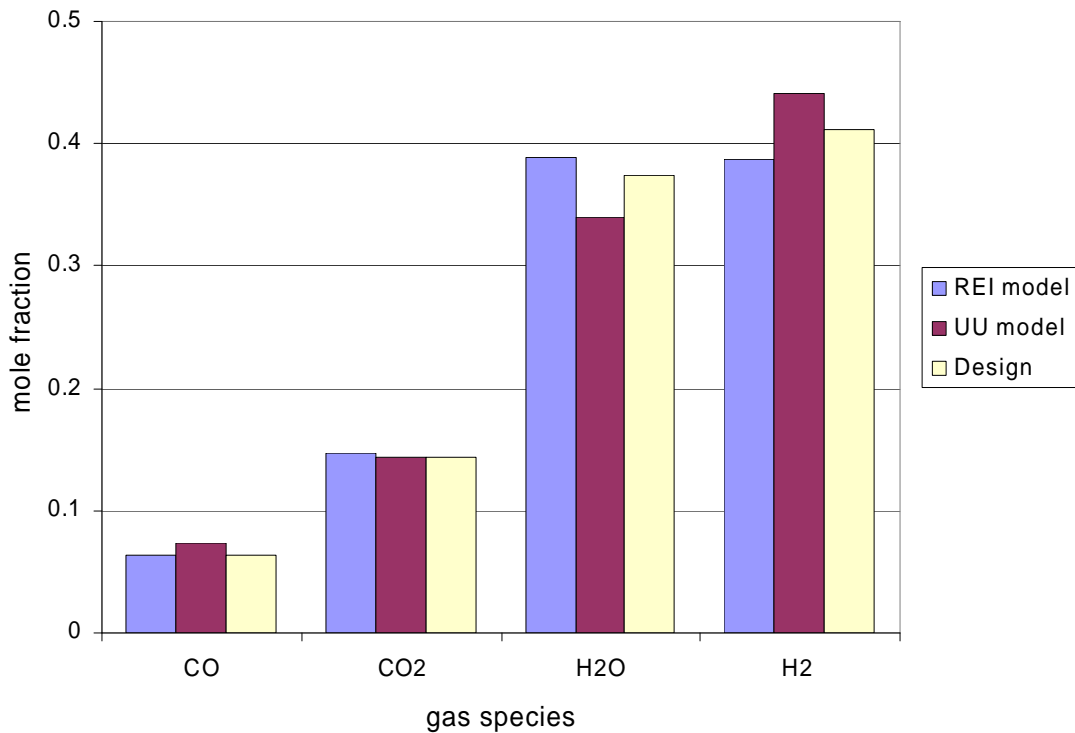


Figure 2. Comparison of syngas composition.

Figure 3 shows the superficial gas velocity and the gas mass flow rate as functions of the reactor height (including the freeboard). A jump increase in both the gas mass flow rate and the superficial gas velocity near the bottom of the fluidized bed is due to the vaporization of black liquor water and pyrolysis of black liquor, after which, the gas mass flow rate increases gradually because of gasification of black liquor. Inside the tube bundles, decreases in the cross-sectional area lead to spikes in the gas velocity. In the freeboard, the gas mass flow rate remains constant, whilst the gas velocity in the freeboard changes because of the expansion of the freeboard and changes in the gas temperature.

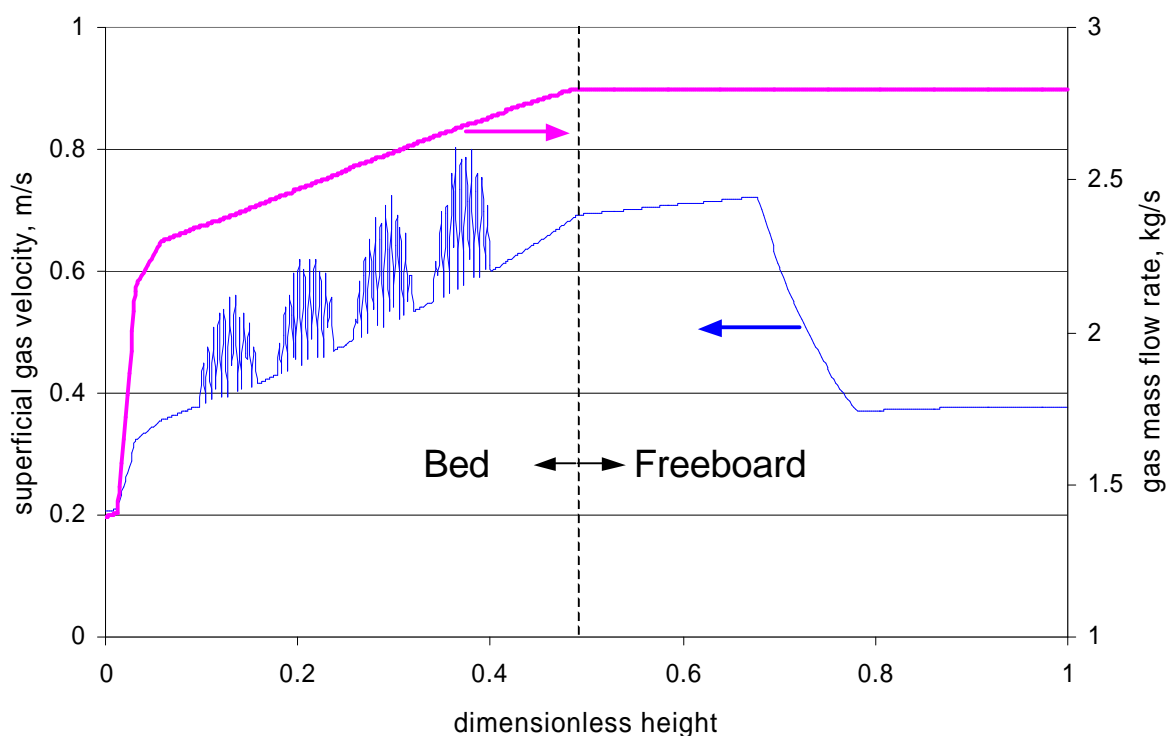


Figure 3. Gas velocity and gas mass flow rate as functions of reactor height.

Figure 4 shows model predicted bubble properties. Inside the tube bundles, bubble size is very small; basically it is the same as the tube pitch. In the open space between the tube banks and the confining cylindrical walls, the maximum bubble size is assumed to be 1/3 of the open space size. In the model calculations, an area-averaged bubble size is used. Also shown in the figure are the bubble sizes for a fluidized bed without any horizontal tubes; for this case, bubbles keep growing along the bed height. The bubble fraction is in the range of 0.15 to 0.4; spikes inside the tube bundles are due to increase in the superficial gas velocity.

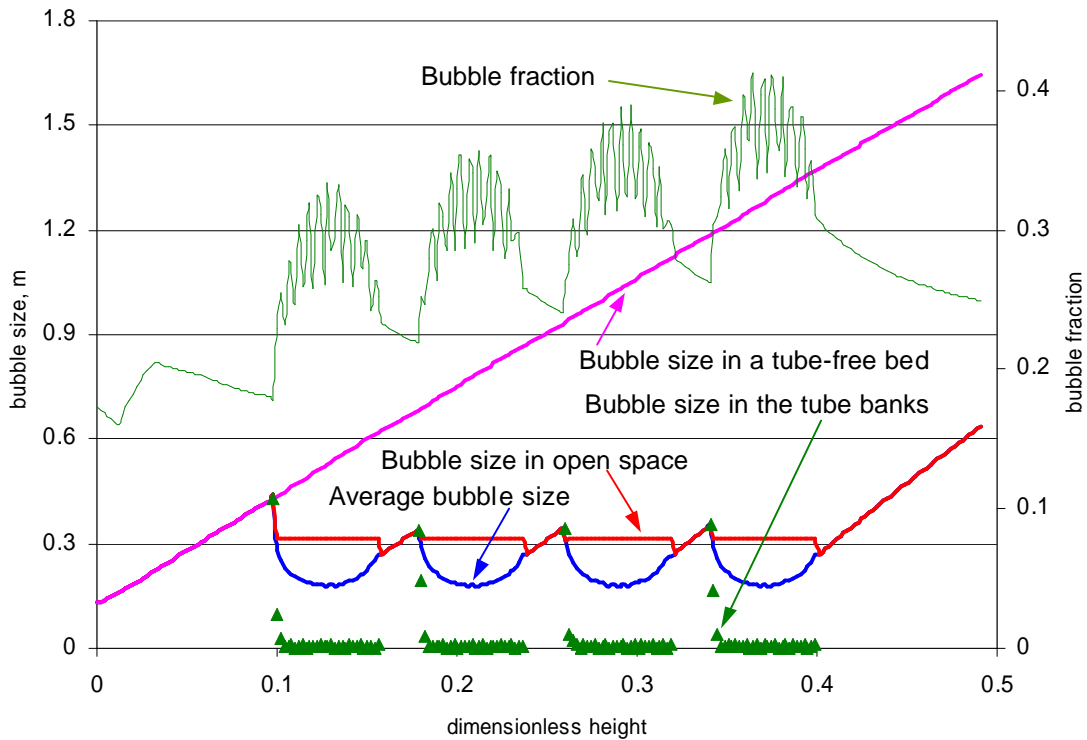


Figure 4. Variation of bubble properties with bed height.

Figure 5 shows gas temperature and particle temperature as functions of the reactor height. It can be seen that particle temperature is essentially the same as the gas temperature; this is not surprising since with a diameter of 300 microns, the solid particles have a very large surface area in contact with the gas phase. A small decrease in the temperature near the bottom of the bed is due to the evaporation of water, followed by a gradual increase in the temperature resulting from heat transferred from the pulse combustors. A marginal decrease in the temperature near the bed surface is due to the endothermic carbon gasification reactions. In the freeboard, there are two major gas phase reactions: the water-gas shift reaction and the methane-water reforming reaction; the former is an exothermic reaction and the latter is an endothermic reaction. The magnitudes of these two reactions dictate the gas temperature. The gas temperature increases in the freeboard because of a higher rate of the water-gas shift reaction. Near the top of the freeboard region, however, the gas temperature decreases slightly due to the endothermic methane-steam reforming reaction. Figure 6 shows variation of gas composition in the fluidized bed. Following a small increase in the black liquor injection point, the water vapor concentration decreases gradually as the gasification proceeds along the height of the bed, while hydrogen and carbon monoxide concentrations increase. In the freeboard, due to the water gas shift reaction, both hydrogen and carbon dioxide concentrations increase and water vapor and carbon monoxide concentrations decrease.

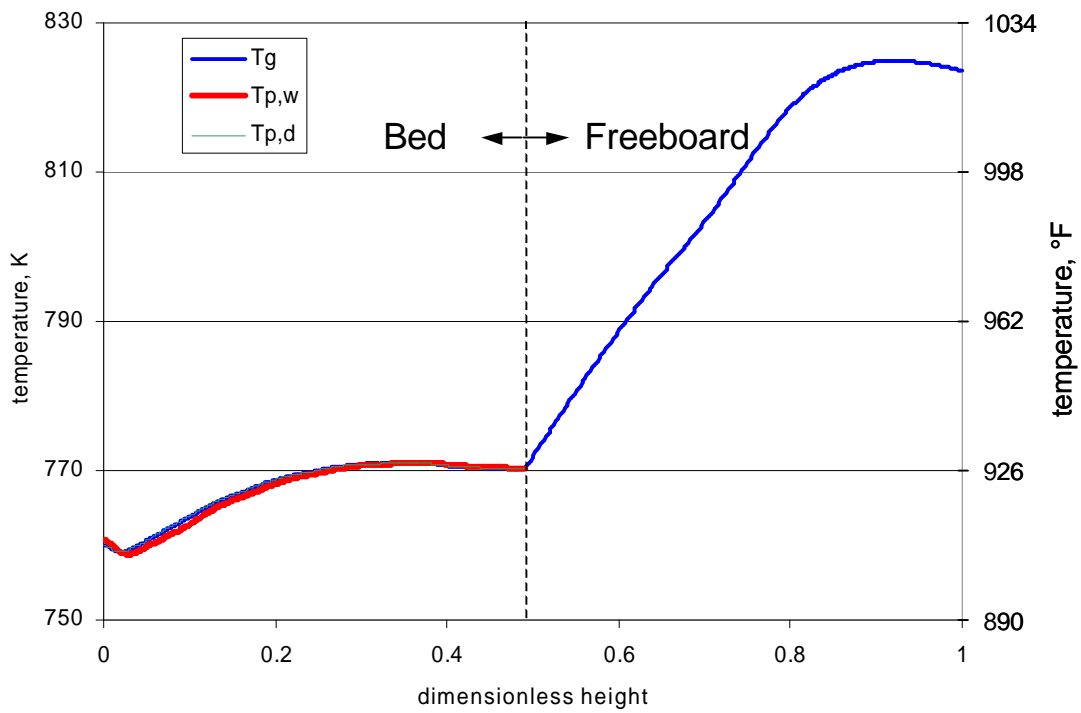


Figure 5. Gas temperature and particle temperature as functions of reactor height.

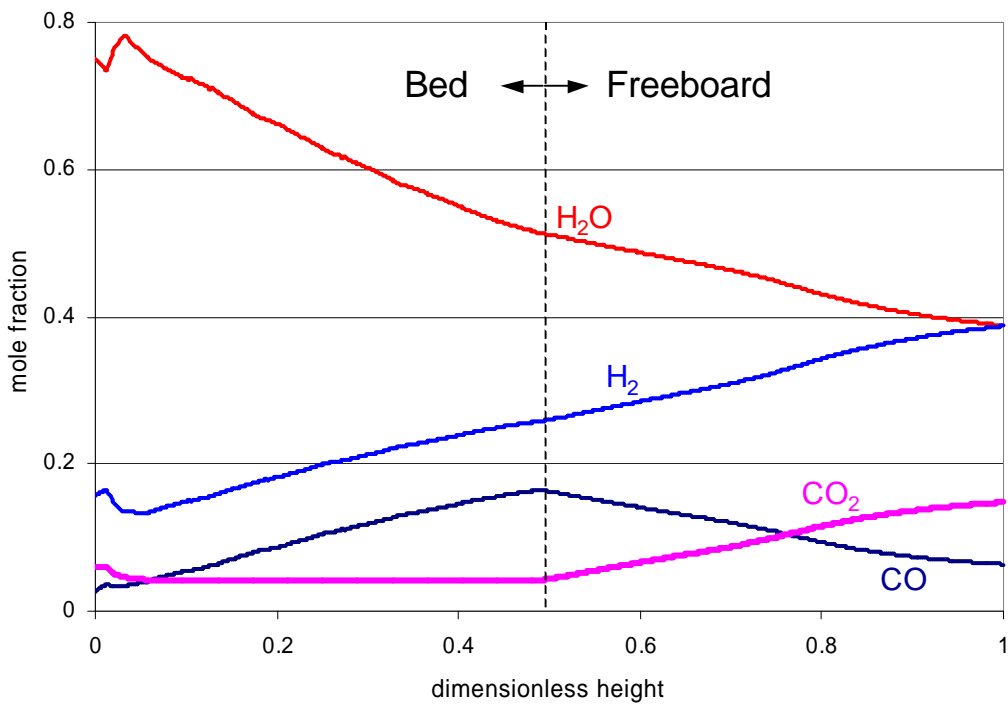


Figure 6. Variation of gas composition with reactor height.

## 5. CONCLUSIONS

A three-phase hydrodynamic model has been developed to simulate black liquor gasification in a commercial demonstration unit consisting of a fluidized bed with horizontal heat exchange tube bundles. Model predicted syngas composition and carbon conversion compare reasonably with available data. Further verification of the model is not possible at present due to lack of experimental data. However, work is in progress on obtaining data under different operating conditions in the commercial demonstration unit and in a laboratory-scale rig. Once the data become available, further validation of the model will be carried out and the influence of operating conditions on the performance of the fluidized bed gasifier will be investigated. The model in its present state is useful in identifying potential problems with the bubble flow through and around tubes, in solids circulation in the bed, and in localized hot spots that might lead to bed agglomeration.

## 6. ACKNOWLEDGEMENTS

The authors would like to thank the DOE for the financial support of this project under a subcontract through the University of Utah (DE-FC26-02NT41490). The DOE project manager is Parrish Galusky. The authors would also like to thank Robert DeCarrera of Georgia-Pacific for his support and Professor Leon Glicksman at MIT for his technical advice.

## 7. NOMENCLATURE

A	cross-sectional area of the bed, $m^2$
C	gas species concentration, $kmol/m^3$
$C_{pg}$	gas specific heat, $J/kg \cdot K$
d	diameter, m
$d_{b,d}$	daughter bubble diameter, m
$d_b$	bubble diameter, m
$d_{b,e}$	average daughter diameter, m
$D_g$	gas diffusivity, $m^2/s$
$D_{O_2}$	oxygen diffusivity, $m^2/s$
f	phase fraction
g	gravitational acceleration, $m/s^2$
h	heat transfer coefficient, $W/m^2 \cdot K$
$H_t$	expanded bed height, m
$K_3$	equilibrium constant
$K_{bw}$	mass transfer coefficient between the bubble phase and the wake phase, 1/s
$K_{wd}$	mass transfer coefficient between the wake phase and the dense phase, 1/s
L	horizontal separation between tubes, m
m	gas mass flow rate, $kg/s$
$M_i$	gas species molecular weight, $kg/kmol$
p	probability
$p_i$	gas species partial pressure, Pa
$Q_t$	heat transferred from the pulse combustor, $W/m^3$
$Q_{vap}$	heat required for evaporation of water, $W/m^3$

R	universal gas constant, J/mol·K
Re	Reynolds number ( $= \rho_g u_{mf} d_p / \mu$ )
$R_{i,b}, R_{i,w,g}, R_{i,d,g}$	homogeneous reaction rate in the bubble, wake and dense phases, kmol/m <sup>3</sup> ·s
$R_{i,w,s}, R_{i,d,s}$	heterogeneous reaction rate in the wake and dense phases, kmol/m <sup>3</sup> ·s
Sc	Schmidt number ( $= \mu / (\rho_g D_g)$ )
T	temperature, K
$u_0$	superficial gas velocity, m/s
$u_b$	bubble rise velocity, m/s
$\varepsilon$	bed voidage
$\varepsilon$	emissivity
$\lambda_{vap}$	latent heat of vaporization, J/kg
$\mu$	gas viscosity, Pa·s
$\rho_g$	gas density, kg/m <sup>3</sup>
$\rho_p$	carbon density, kg/m <sup>3</sup>
$\sigma$	Stefan-Boltzmann constant
$\Delta H$	heat of reaction, J/kmol

### *Subscripts*

ash	ash in black liquor
b	bubble phase
bed	bed
c	carbon
d	dense (emulsion) phase or daughter bubble
f	freeboard or film
g	gas
i	gas species index
inlet	inlet conditions
j	cell index
mf	minimum fluidization
p	particle
s	solids
t	tube
w	wake phase

## **8. REFERENCES**

Chen Z., Lin M., Ignowski J., Kelly B., Linjewile T.M. and Agarwal P.K., Mathematical modeling of fluidized bed combustion 4. N<sub>2</sub>O and NO<sub>x</sub> emissions from the combustion of char, *Fuel*, **80**, 1259-1272 (2001).

Darton R.C., La Nauze R.D., Davidson J.F. and Harrison D., Bubble growth due to coalescence in fluidized beds, *Trans. IChemE*, **55**, 274-280 (1977).

Dayton D.C. and Frederick W.J., The direct observation of alkali vapor release during biomass combustion and gasification 2. Black liquor combustion at 1100°C, *Energy and Fuels*, 1996.

Davidson J.F. and D. Harrison D., *Fluidized Particles*, Cambridge University Press, London, 1963.

DeCarrera R., Ohl M., Robertson D. and Gemmer R., Engineering study for a full scale demonstration of steam reforming black liquor gasification at Georgia-Pacific's mill in Big Inland, Virginia, Final Report, DE-FC07-99ID13818, 2002.

Desai P.R. and Wen C.Y., Computer modeling of the MERC fixed bed gasifier, MERC/CR-78/3, 1978.

Frederick W.J., Combustion processes in black liquor recovery: analysis and interpretation of combustion rate data and an engineering design model, DOE Report, DOE/CE/40637-T8 (DE90012712), March, 1990.

Frederick W.J. and Hupa M., Combustion properties of kraft black liquors, DOE Report, DOE/CE/40936-T1, Washington D.C., 1993.

Frederick W.J., Iisa K., Wåg K.J., Reis V.V., Boonsongsup L., Forssén M. and Hupa M., Sodium and Sulfur Release and Recapture During Black Liquor Burning, DOE Report, DOE/CE/40936-T2, 1995.

Fryer C. and Potter O.W., Experimental investigation of models for fluidized bed catalytic reactors, *AIChE J.*, **22**, 38-47 (1976).

Grace and Timmer, A comparison of alternative black liquor recovery technologies, *TAPPI Proceedings, 1995 Int. Chemical Recovery Conference*, Atlanta, USA, 1995.

Guenther C., Shahnam M., Syamlal, M., Longanbach J., Cicero D. and P.V. Smith, CFD modeling of a transport gasifier, 19<sup>th</sup> Annual Pittsburgh Coal Conference, September 23-27, 2002.

Gunn D.J., Transfer of heat or mass to particles in fixed and fluidized beds, *Int. J. Heat Mass Transfer*, **21**, 467-476 (1978).

Hull A.S., Chen Z., Fritz J.W. and Agarwal P.K., Influence of horizontal tube banks on the behavior of bubbling fluidized beds. I. Bubble hydrodynamics, *Powder Technology*, **103**, 230-242 (1999).

Jones W.P. and Lindstedt R.P., Global reaction schemes for hydrocarbon combustion, *Combustion and Flame*, **73**, 233-249 (1988).

Kunii D. and Levenspiel O., *Fluidization Engineering*, 2<sup>nd</sup>, John Wiley & Sons, New York, 1991.

Li J. and van Heiningen A.R.P., Kinetics of CO<sub>2</sub> gasification of fast pyrolysis black liquor char, *Ind. Eng. Chem. Res.*, **29**, 1776-1785 (1990).

Li J. and van Heiningen A.R.P., Kinetics of gasification of black liquor char by steam, *Ind. Eng. Chem. Res.*, **30**, 1594-1601 (1991).

Lim K.S., Gururajan V.S. and Agarwal P.K., Mixing of homogeneous solids in bubbling fluidized beds: Theoretical modeling and experimental investigation using digital image analysis, *Chem. Eng. Sci.*, **48**, 2251-2265 (1993).

Peters N., Premixed burning in diffusion flames - the flame zone model of Libby and Economos, *Int. J. Heat Mass Transfer*, **22**, 691-703 (1979).

Rowe P.N. and Partridge B.A., An X-ray study of bubbles in fluidized beds, *Trans IChemE*, **43**, 157-175 (1965).

Rowe P.N. and Yacono C.X.R., The bubbling behavior of fine powders when fluidized, *Chem. Eng. Sci.*, **31**, 1179-1192 (1976).

Syamlal M. and Bissett L.A., METC gasifier advanced simulation (MGAS) model, Technical Note, NTIS report No. DOE/METC-92/4108 (1992).

Verrill C.L. and Wessel R.A., Sodium loss during black liquor drying and devolatilization – application of modeling results to understanding laboratory data, *Proceedings of 1995 Int. Chem. Recovery Conference*, Toronto, April 23-27, B89-B103 (1995).

Wen C.Y., Chen H. and Onozaki M., User's manual for computer simulation and design of the moving bed coal gasifier, DOE/MC/16474-1390, NTIS/DE83009533, 1982.

Werther J., Bubble growth in large diameter fluidized beds, in D.L. Kearins (ed) *Fluidization Technology, Vol. I*, Hemisphere, 1976, 215-235 (1976).

Westbrook C.K. and Dryer F.L., Simplified mechanisms for the oxidation of hydrocarbon fuels in flames, *Combustion Sci. Tech.*, **27**, 31-43 (1981).

Whitty K., Investigation of fuel chemistry and bed properties in a fluidized bed black liquor steam reformer, DOE Project Quarterly Report, DE-FC26-02NT41490, 2003.

Yates J.G. and Ruiz-Martinez R.S., Interaction between horizontal tubes and gas bubbles in a fluidized bed, *Chem. Eng. Comm.*, **62**, 67-78 (1987).

Yates J.G., Ruiz-Martinez R.S. and Cheesman D.J., Prediction of bubble size in a fluidized bed containing horizontal tubes, *Chem. Eng. Sci.*, **45**, 1105-1115 (1990).